Monolithically Integrated Silicon-IMPATT Oscillator at 93 GHz

C. Schöllhorn[1], M. Morschbach[1], M. Oehme[1], J. Hasch[2], H. Irion[2] and E. Kasper[1]

[1] : Institut für Halbleitertechnik, Universität Stuttgart, Pfaffenwaldring 47, 70569 Stuttgart, Germany
[2] : Robert Bosch GmbH, Corporate Research and Development, FV/FLO, Robert-Bosch-Platz 1, 70839 Gerlingen, Germany

Abstract — **In this paper monolithically integrated IMPATT diodes are presented. To prove the concept of completely monolithic integration, no special heatsinks or other constructions to optimize cooling were used. The diodes were grown with molecular beam epitaxy on a high resistivity silicon substrate. S-Parameter measurements were performed from 85 GHz up to 110 GHz, showing high negative impedances above the avalanche frequency. Oscillations at a frequency near 93 GHz were observed with the designed resonator circuit.**

I. INTRODUCTION

In the last few years Silicon Monolithic Millimeter Wave Integrated Circuits, so called SIMMWICs, got more and more important because of their high reliability, low cost and increasing performance [1],[2] and [3]. In some early publications [4],[5] integrated Si-Impatt diodes are described, because they are able to produce high RF output power at frequencies above 90 GHz. Impatt diodes are near their thermal limit because they are always operated in the avalanche breakdown. To avoid the destruction of the diodes, immense technical effort was undertaken to provide the diodes with effective cooling. In most cases the diodes are thermocompressed on diamond heatsinks as performed in the work of Dalle [6] and Wollitzer [7] for example. In this case the diodes are manufactured with beam leads to provide good electrical contact and to achieve mechanical stability. Unfortunately all these processes are not stable enough, time-consuming and not compatible with state of the art integration techniques because of the required manual work. This leads to a very low production yield and prevents cost effective realization. An advancement in integrating and housing Impatt diodes is presented in [8]. Luschas replaced the sensitive beam leads by a thick metal layer. This simplifies and ensures the time consuming bonding process but nevertheless a manual bonding step has to be performed. According to this very special technology he has to use a SIMOX wafer and is constrained to perform backside photolithography. In this paper we present completely monolithically integrated planar Impatt-diodes manufactured with process steps very close to a standard process. The oscillator is realized using a coplanar waveguide resonator circuit. For additional DC and S-parameter measurements, some Impatt diodes are integrated in coplanar waveguide (CPW) test structures.

II. TECHNOLOGY

As substrate we used float zone (FZ) silicon p^{--} wafers with a high specific resistivity >1000 Ωcm. The active layers are grown with molecular beam epitaxy (MBE). This allows the sharp transitions (more than 3 orders of magnitude) in the doping level. The MBE grown layer stack can be seen in figure 1.

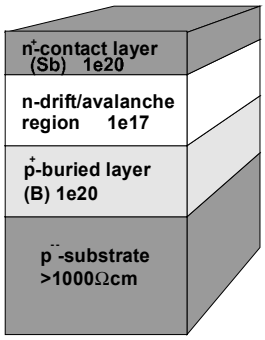

Fig. 1. Layer stack of an integrated IMPATT diode grown with molecular beam epitaxy.

The process starts with a mesa etch step to make the contact to the high p-doped buried layer. The second step, a trench etching step, isolates the diodes from each other and uncovers the high resistivity silicon of the substrate to reduce the RF attenuation of the coplanar resonator. In a third step the isolating silicon oxide is deposited and the contact holes are etched. In the last step the aluminum metalization is sputtered and patterned. The process is described in more detail in [9]. Fig. 2 shows a scanning electron microscope (SEM) picture of a processed Impatt diode, integrated into aluminum coplanar waveguides.

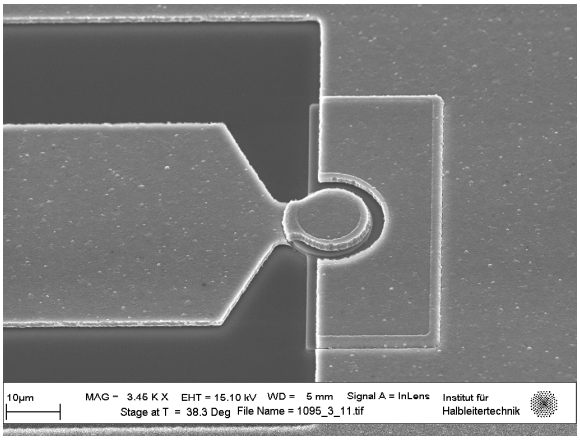

Fig. 2. Scanning electron microscope (SEM) picture of a monolithically integrated IMPATT diode connected to a coplanar waveguide.

III. DC AND RF MEASUREMENTS

The IV-curve of an Impatt-Diode is shown in fig. 3. For Impatt diodes the reverse current of the IV-curve is the interesting part, because Impatt diodes are operated in the avalanche breakdown. To obtain good performance a very small reverse current, in our case <1.0exp^{-11} A (U=-1 V), and a well defined, reproducible breakdown are necessary.

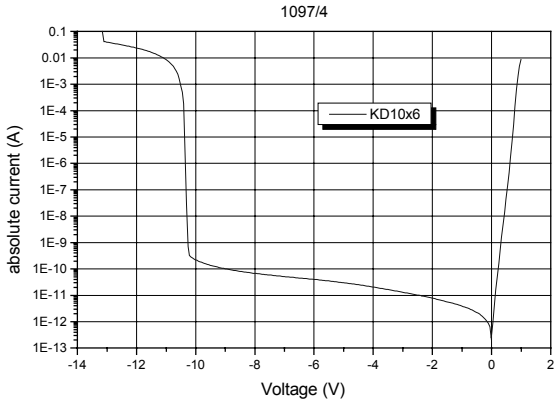

Fig. 3. IV-curve and break-through of the IMPATT diodes. The break-through voltage is 10.4 V.

Impatt diodes are able to oscillate at frequencies above the avalanche frequency f_a, because in this frequency range the real- and imaginary part of the diode impedance are both negative [10]. To characterize the diode impedances, some diodes are integrated into a coplanar waveguide (fig. 4).

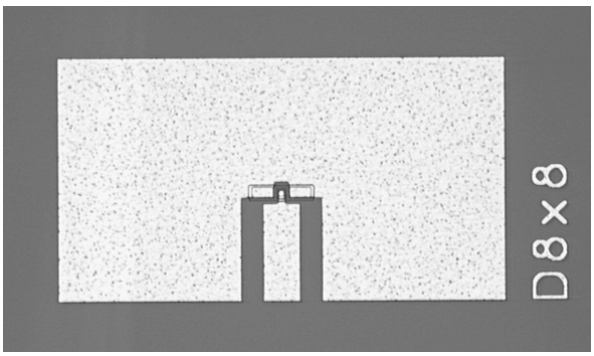

Fig. 4. Picture of the Impatt diode embedded into a coplanar waveguide for S-parameter measurements.

In a first step the reflection coefficient of the integrated diodes is measured. The frequency range is 85 GHz to 110 GHz. Thereafter the reflection coefficient r is transformed into the impedance using the formula given in equation (1) with the characteristic wave impedance Z_0=50 Ω.

$$Z = \frac{1+r}{1-r} \cdot Z_0 \qquad (1)$$

In a last step a deembedding procedure is performed to subtract the parallel and series parasitics caused by the CPW. To perform the deembedding procedure an open and a short structure with the same layout are measured additionally. The impedance of the inner diode Z_{diode} can be calculated with the following equation :

$$Z_{diode} = (Y_{dut} - Y_{open})^{-1} - (Y_{short} - Y_{open})^{-1} \qquad (2)$$

Y_{dut} is the measured Y-parameter of the complete structure including the active device while Y_{short} and Y_{open} are Y-parameters of the short circuit and the open circuit respectively. The deembedding procedure is described in more detail in [11].

Fig. 5 shows the impedance of the 8*8µm²-diode after deembedding for several reverse currents up to a maximum of 35 mA. The current density increases from 0.312 mA/µm² for a reverse current of 20 mA to 0.547 mA/µm² for a reverse current of 35 mA. According to equation (3) which describes the dependency of the avalanche frequency f_a from the current density J_0 [12], this leads to an increasing avalanche frequency.

$$f_a = \frac{1}{2\pi} \cdot \sqrt{\frac{2\alpha' \cdot \upsilon_s \cdot J_0}{\varepsilon}} \qquad (3)$$

α' : differential of the ionisation coefficient with respect to the electric field
ε : semiconductor permittivity
υ_s : saturation velocity

Because the measurement setup we used has a minimum frequency of 85 GHz it is not possible to determine the exact avalanche frequency from the S-parameter measurements. Extrapolations of the impedance curves give avalanche frequencies between 46 GHz and 60 GHz for the current range 20 mA to 35 mA. The avalanche frequencies for the different current densities are summarized in table 1.

	Reverse current			
	20mA	25mA	30mA	35mA
J_0 [mA/µm²]	0.312	0.390	0.469	0.547
f_a [GHz]	46	51	56	60

TABLE I
AVALANCHE FREQUENCY IN DEPENDENCY OF THE REVERSE CURRENT

Because the differential of the ionization coefficient and the saturation velocity in equation (3) decrease with increasing temperature and thus increasing current density, the avalanche frequency increases slower than the square root of the current.

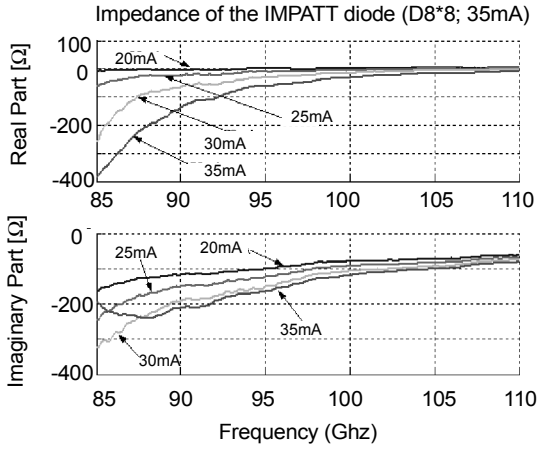

Fig. 5. Real- and imaginary part of the diode impedance above the avalanche frequency for different current densities.

A more detailed look at the impedance level around the oscillation frequency (93 GHz) reveals high negative real- and imaginary values. From fig. 6 a value of –170 Ω for the imaginary part and -48 Ω for the real part can be read off. The very high negative impedance of the integrated Impatt diode allows a simple resonator circuit design for a first oscillator test.

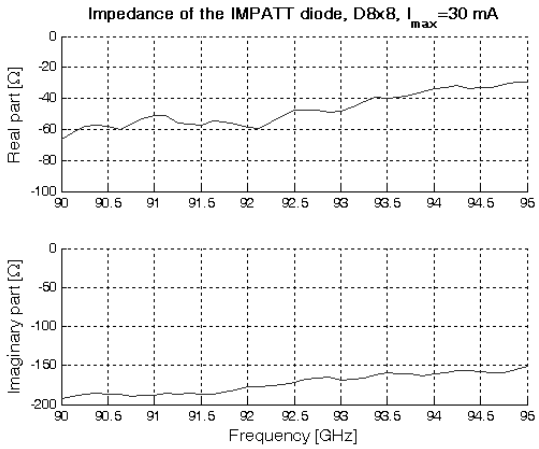

Fig. 6. Real- and imaginary part of the impedance around the oscillating frequency.

IV. DESIGN OF THE RESONATOR

In order to allow diode oscillations a series of resonators with adapted impedances were designed. As design tool we used Microwave Studio from CST®. The impedance of the diodes is determined with the S-parameter measurements described in section III. Fig. 7 shows a photograph of the resonator. In this case a rectangular diode with a size of 8 µm*8 µm was embedded. The left side of the picture shows the contact for the GSG prober head. Simultaneously the RF tips are used to bias the device into the breakdown. On the right side the coplanar waveguide, with a length of λ/4, builds a short circuit. This short circuit is transformed into an open circuit by the CPW. From the view of the diode this open structure builds the resulting impedance of the resonator. Fig. 8 shows the spectrum of the oscillating Impatt diode at an operating current of 30 mA. The reverse voltage is increased to -12.9 V because of the temperature coefficient of the avalanche breakdown (see also upper curve portion in fig. 3). This leads to an oscillating frequency of 93 GHz which proves the functionality of completely monolithically integrated silicon Impatt diodes.

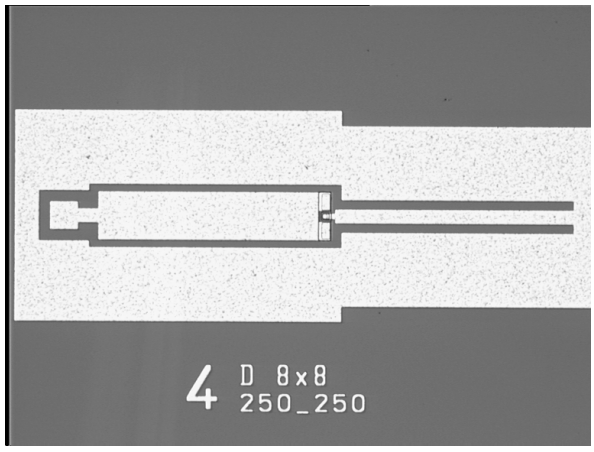

Fig. 7. Photograph of the resonator with an embedded 8*8µm² IMPATT diode.

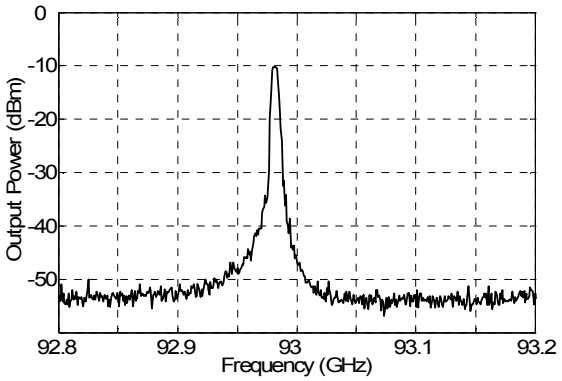

Fig. 8. Output power spectrum of the IMPATT diode oscillator at 92.98 GHz.

V. CONCLUSION

The presented results show the feasibility of manufacturing completely monolithically integrated silicon IMPATT diodes. The high frequency characterization of the diode behavior above avalanche frequency was carried out by S-parameter measurements. Together with the designed planar resonator circuit, oscillations at frequencies above 90 GHz were observed. The next step will be improving the output power of the oscillator. This can be achieved by modifying the resonator circuit design, thereby allowing a large signal operation mode.

ACKNOWLEDGEMENT

Financial support from Deutsche Forschungs-gemeinschaft (DFG) under contract no. Ka 1229/4-1 and Ka 1229/4-2 is acknowledged.

REFERENCES

[1] Luy, J.-F. and P. Russer, *"Silicon Based Millimeter-Wave Devices",* Springer Verlag, Berlin, 1994.

[2] Beck, D., M. Herrmann, E. Kasper, *"CMOS on FZ-High-Resistivity Substrate for Integration of SiGe-RF-Circuitry and Readout Electronics"*, IEEE Trans. on Electron Devices, ED-44, pp. 1091-1101, 1997.

[3] Strohm, K.M., J. Buechler, E.Kasper, *"SIMMWIC Rectennas on High-Resistivity Silicon and CMOS Compatibility"*, IEEE Trans. MTT-46, pp. 669-676, 1998.

[4] Stiller, A., E.M. Biebl, J.-F. Luy, K.M. Strohm and J. Buechler, *"A Monolithic Integrated Millimeter Wave Transmitter for Automotive Applications"*, IEEE Trans. Microwave Theory Tech., Vol. 43, No. 7, pp. 1654-1658, 1995.

[5] Buechler, J., K.M. Strohm, J.-F. Luy, T. Goeller, S. Sattler and P. Russer, *"Coplanar Monolithic Silicon Impatt Transmitters"*, Proc. of the 21st Europ. Microwave Conf., Stuttgart, pp. 352-357, 1991.

[6] Dalle, C., P.-A. Rolland and G. Lleti, *"Flat Doping Profile Double-Drift Silicon Impatt for Reliable CW High-Power High Efficiency Generation in the 94GHz Window"*, IEEE Trans. on Electron Devices, Vol. 37, No. 1, pp. 227-236, 1990.

[7] Wollitzer, M, *"Planare Silizium-IMPATT-Oszillator-schaltungen bei 140GHz"*, Fortschritt-Berichte VDI, Nr. 286, VDI-Verlag, Düsseldorf, 1998.

[8] Luschas, M., R. Judaschke and J.-F. Luy, *"Simulation and Measurement of 150GHz Integrated Silicon Impatt Diodes"*, Proc. of the IEEE Microwave Theory and Tech. Symp., Seattle, pp. 1269-1272, 2002.

[9] Schöllhorn, C., W. Zhao, M. Morschbach, M. Oehme, E. Kasper, J. Hasch and H. Irion, *"100GHz S-Parameter Measurements of Monolithically Integrated Silicon Impatt Diodes"*, Proc. of the Asia Pacific Microwave Conf. Kyoto, 2002.

[10] Unger, H.-G., and W. Harth, *"Hochfrequenz-Halbleiterelektronik"*, S. Hirzel Verlag, Stuttgart, 1972.

[11] Koolen, M.C.A.M., J.A.M. Geelen, M.P.J.G. Versleijen, *"An Improved De-Embedding Technique for On-wafer High-frequency Characterization"*, IEEE Bipolar Circuits and Technology Meeting, vol. 1, pp. 188-191, 1991.

[12] Sze, S. M., *Physics of Semiconductor Devices,* John Wiley & Sons, New York, 1969.